

Evolutionary timeline of a modeled cell

Vrani Ibarra-Junquera
*Laboratorio de Agrobiotecnología,
Universidad de Colima,
Coquimatlán, C.P. 28400, Colima, México.*

Diego Radillo-Ochoa* and César A. Terrero-Escalante
*Facultad de Ciencias, Universidad de Colima, Bernal Díaz del Castillo 340,
Col. Villas San Sebastián, C.P. 28045, Colima, Colima, México.*

(Dated: January 26, 2022)

A theoretical study of cell evolution is presented here. By using a toolbox containing an intracellular catalytic reaction network model and a mutation-selection process, four distinct phases of self-organization were unveiled. First, the nutrients prevail as the central substrate of the chemical reactions. Second, the cell becomes a *small-world*. Third, a highly connected core component emerges, concurrently with the nutrient carriers becoming the central product of reactions. Finally, the cell reaches a steady configuration where the concentrations of the core chemical species are described by Zipf's law.

Keywords: metabolic networks; cell evolution; graph theory; origin of life.

I. INTRODUCTION

A key goal of postgenomic cell biology is to understand the cellular organization at its core functional level. As a result of ongoing efforts in genome sequencing, a large number of highly complex intracellular networks have been completely mapped out, revealing common features not only among all living organisms, but also among other natural and even human-made networks. These findings lead to the search for the fundamental organizational mechanisms that have shaped the evolution of life as we currently know it. A complete introduction to this topic can be found in Ref. [1], where most of the technical terminology used in this paper is explained.

Analyzing complex biological networks on a top-down approach (from the observational uncovering of the cell structure to the determination of the specific role of each element) is a burdensome task, since the vast diversity and specificity of components, along with their physical size scale, makes unveiling the organizational principles difficult. A key issue here is that, with current imaging techniques, dynamics inside living cells remain largely inaccessible at molecular level. Even more, though big steps are being made in this direction [2], since these systems have been developing over a billion of years of evolution, this kind of analysis is constrained by the time at which the networks are sampled, limiting insight into their evolutionary history. Efforts are also being done to overcome this time constraint, such as inferring ancestral metabolic networks using methods to estimate the genetic distance between different bacterial species as given by phylogenetic trees built following the maximum parsimony criterion [3], and also using structure-guided

sequence analysis of proteins to explore the patterns of evolution of enzymes responsible for biogeochemical cycles [4].

A fruitful way to address the limitations mentioned above is by adopting the philosophy which considers the cell as the “minimal unit of life”, i.e., a self-sustaining chemical system capable of undergoing Darwinian evolution [5, 6]. This simple cell can be studied by means of mathematical models that describe aspects of the cell in a bottom-up approach. The theoretical study of cellular behavior can be traced back over 50 years to the pioneering works of Kauffman [7], in which cell complexity is studied from the perspective of random mathematical networks. His works belong in the wider context of contemporary network theory, which is marked by the discoveries of surprising similarities among the structures of a wide variety of real systems coming from seemingly unrelated areas. Over the past 20 years, this branch of biology has experienced an accelerated growth steered by technological advances that have led, among other advantages, to an easier accessibility to higher computational power. As a result, several mathematical models have been proposed and thoroughly studied, like the simple boolean gene-interaction networks [8], the condensation-cleavage binary polymer model [9] or the evolutionary process based on an artificial chemistry of catalysed reactions proposed in [10]. This kind of simulations have proved to be useful for providing insights into the underlying principles of cell evolution.

In this work we used a cellular model based on catalytic reaction networks, which are modified as a result of a Darwinian-like evolutionary process of mutation and selection. A version of the model was first proposed in 1997 by Kaneko and Yomo [11], while the corresponding evolutionary process was introduced in 2006 by Furusawa and Kaneko [12]. This model differentiates itself from the rest because its dynamics are given by a system of ordinary differential equations that describe the enzymatic

* Author names are arranged alphabetically. Corresponding author: dradillo1@ucol.mx

kinetics of a complex network of unspecified chemical components which includes passive diffusion of nutrients into the cell from the environment. Additionally it is important to point that, by including the evolutionary process, the focus ceases to be on the behavior of a single cell, and instead the role of the competition among groups of cells is observed, which ultimately serves as the external input driving the self-optimization process inside a cell. In previous works it has been shown that different versions of this model are able to reproduce well-known characteristics of living cells, giving insights into cellular processes such as differentiation [13], pluripotency [14] and reaction to environmental perturbations [15].

The main goal of our work is to use the well suited set of tools from graph theory to provide a basic but comprehensive analysis of the evolution of the reaction network during the mutation-selection process, as described by a particular version of the Kaneko-Yomo model. We confirmed that a self-reproducing system of cells can arise from the simple rules considered in the model and in the evolutionary process. Beyond that, our analysis of the changes in the topology of the reaction networks reveals striking similarities with real metabolic networks and also provides new insights into the events that could have occurred in the earlier stages of life development. Our results are summarized in Fig. 12, which displays the evolutionary timeline of the modeled cell as determined by the mutation-selection process. Motivated by these results, this manuscript is also meant to serve as groundwork for future research using versions of the model and evolutionary process. With this aim, in sections II to IV, we provide a detailed derivation of the expressions for the enzymatic kinetics and the cellular growth rate, as well as a description of our computational implementation of single-cell dynamics and the simulation of the evolutionary process. This way are filled key voids we have found in the literature about the version of the model we use. Our results are then addressed in section V. Finally, this paper ends in section VI, with the presentation and discussion of our conclusions.

II. MODEL OF THE INTRACELLULAR CHEMISTRY

As mentioned in the Introduction, our research is enclosed in the conceptual framework where a cell is defined as a self-sustaining chemical system capable of undergoing Darwinian evolution. As the mathematical model for the internal dynamics of such simple cell, we use the catalytic reaction network model described in Ref. [12]. In this section we provide a detailed derivation of the corresponding ordinary differential equations, which seems to be missing elsewhere in the literature.

Let us start by considering the set of variables $\{n_0, n_1, \dots, n_N\}$, which represent the number of molecules of each of the N chemical species that exist within a cell. In general, the volume of a cell changes due to variations

in intracellular solute content or extracellular osmolality. Without loss of generality, in this model we assume that cellular volume is proportional to the total number of molecules inside the cell, that is,

$$V = \alpha \sum_i n_i, \quad (1)$$

where α is the proportionality constant. Therefore, the intracellular concentration of the species i is given by

$$x_i = \frac{n_i}{V}, \quad (2)$$

such that the internal cellular state can be described by the concentration vector $\mathbf{x} = (x_0, x_1, \dots, x_N)$. The rate of change in time t of x_i is then given by

$$\begin{aligned} \frac{dx_i}{dt} &= \frac{1}{V} \frac{dn_i}{dt} - n_i \frac{1}{V^2} \frac{dV}{dt} \\ &= \frac{1}{V} \frac{dn_i}{dt} - x_i \frac{1}{V} \frac{dV}{dt}. \end{aligned} \quad (3)$$

Let us define

$$R_i \equiv \frac{1}{V} \frac{dn_i}{dt}, \quad (4)$$

$$C_i \equiv -x_i \frac{1}{V} \frac{dV}{dt}, \quad (5)$$

such that

$$\frac{dx_i}{dt} = R_i + C_i. \quad (6)$$

Note that R_i is related to the change in the amount of molecules of the species i , whereas C_i relates to the overall change in cellular volume.

In this model, the number of molecules of each species as a function of time is determined by the dynamics of a catalytic reaction network. Reaction kinetics are assumed to be described by the law of mass action in steady state. For simplicity, the only interaction between the environment and the cell considered in this model is the passive diffusion of a few species through the cell membrane. From now on these permeable species are referred as *nutrients*, and their diffusion is aided by specific *carrier* species. With these considerations, R_i is defined as

$$\begin{aligned} R_i(\mathbf{x}) \equiv & \sum_{j,l} \sigma_{j,i,l} x_j x_l - \sum_{j',l'} \sigma_{i,j',l'} x_i x_{l'} \\ & \left(+ D x_{m_i} (x_i - x_i) \right), \end{aligned} \quad (7)$$

where the first two terms represent the enzymatic kinetics involving the species i as product or substrate, with each reaction correspondingly catalyzed by the species l and l' . The factor $\sigma_{i,j,l}$ is equal to 1 if reaction $i + l \rightarrow j + l$ takes place, and 0 otherwise. The third term is written in parentheses to denote that it is only added to the equations of the nutrient species to include the corresponding diffusion process with coefficient D and its respective

carrier x_{m_i} . It is worth emphasizing that considering the role of a carrier species results in an effective time dependent diffusion coefficient, which allows the cell to self-regulate its exchange of nutrients with the environment.

Next, in order to express C_i in terms of the vector \mathbf{x} , let us consider the derivative of Eq. (1),

$$\frac{dV}{dt} = \alpha \sum_j \frac{dn_j}{dt}. \quad (8)$$

Multiplying both sides by $-x_i/V$ and substituting the definition of R_i and C_i , we obtain

$$C_i(\mathbf{x}) = -\alpha x_i \sum_j R_j. \quad (9)$$

Finally, the rate of change for the intracellular concentration of a species i can be expressed as

$$\frac{dx_i}{dt} = R_i - \alpha x_i \sum_j R_j. \quad (10)$$

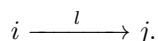
In the case $\alpha = 1$, this equation corresponds to the one presented in Ref. [12].

Typically, a large number N of species is considered in the model, therefore the solutions to the above system must be obtained numerically. We do this by approximating R_i using an implementation of the fourth order Runge-Kutta method for many variables. Although sophisticated multi-step methods offer higher accuracy of the numerical approximation, with reasonable increase in the computational requirements, we have chosen the relatively simple Runge-Kutta method, taking into account that Eq. (2) provides a convenient test for accuracy of our numerical results; identity

$$\sum_i x_i = \frac{1}{\alpha}, \quad (11)$$

must always be satisfied during the whole cell evolution. The value of α is established by the selection of the initial conditions for the concentrations.

As mentioned before, the dynamics of the concentrations of the different chemical species are dictated by a catalytic reaction network. Let us now describe the mathematical representation we used to model it. The reaction network can be represented by a *directed graph*, a mathematical object consisting of a set of *nodes* connected by *edges* that have a definite direction. Each node in the network corresponds to a different chemical species. A pair of nodes is connected by an edge if there is a reaction that involves its respective species either as subtract or product. The edge will be directed towards the node corresponding to the product of the reaction. Every edge possesses an attribute associated with the catalyst of the reaction it represents. Schematically, a reaction in this network could be represented as



The structure of this graph additionally complies with a number of biologically inspired constraints. As we will see in the following sections, cell growth is central to our study, considering it to be due to biosynthesis processes, reactions on the network are set to occur on a single direction; such that there are no symmetric pairs of directed edges, restricting its structure to one of an *oriented graph*. Moreover, the nutrient species are not allowed to be product of any intracellular reaction, so that they only grow by permeating to the cell from the environment. Also, since facilitated diffusion typically involves the transport of ions and polar molecules such as carbohydrates and amino acids, nutrients are not used in this model as catalyst enzymes for any reaction. Neither are nutrient carriers, due to their specific role. With these constraints, the catalyst for each reaction is chosen randomly from the set of all available catalysts, verifying that the reactions satisfy a one-to-one correspondence from the substrate-catalyst pair $i+l$ to the product-catalyst pair $j+l$, where $l \neq i, j$.

Let us end this section by recalling that the binary fission time of a cell strongly depends on the organism and even in the given tissue of a multicellular organism. It varies over a broad range spanning from minutes to years. Taking this into account, in Eqs. (10) we are using dimensionless time.

III. CELL GROWTH RATE

Cellular growth rate plays a central role in this work. Following Ref. [12], it is defined as the inverse of the duplication time t_d , i.e., the time it takes for a cell to double its initial volume. Recall that in this model the volume is proportional to the number of molecules inside the cell (see Eq. (1)). However, the dynamic variables used in Eqs. (10) are the concentrations of the different chemical species within the cell, \mathbf{x} , which are in turn determined by the cellular volume, as seen in Eq. (2). As a consequence, any attempt to combine these equations to obtain an expression for the volume in terms of the concentrations results in an inconsistent system. Therefore, to obtain an expression to determine t_d becomes non trivial. The expression to calculate the growth rate we use here is different from the one given in Ref. [16]. and the related literature. To derive it, let us start by rewriting Eq. (8) as follows,

$$\frac{dV}{V} = \alpha \sum_j R_j(\mathbf{x}) dt. \quad (12)$$

This expression can be integrated over a time interval t_0 to t ,

$$\ln \frac{V_t}{V_0} = \alpha \int_{t_0}^t \sum_j R_j(\mathbf{x}) dt. \quad (13)$$

where V_0 is the initial cellular volume and V_t is its value at time t . Since at $t = t_d$ the volume is $V_t = 2V_0$, the

condition for the duplication time becomes,

$$\alpha \int_{t_0}^{t=t_d} \sum_j R_j(\mathbf{x}) dt = \ln 2. \quad (14)$$

In our work $R_j(\mathbf{x})$ is calculated from the numerical approximation for the temporal evolution of \mathbf{x} , as mentioned in Sec. II. This means that the definite integral in Eq. (14) must be numerically approximated as well. In our implementation, this is done using the composite Simpson's rule, where an approximation S to the value of an integral is calculated using $s+1$ equally spaced points with a step size h over a given time interval (t_i, t_f) as

$$\begin{aligned} \int_{t_i}^{t_f} \sum_j R_j(\mathbf{x}) dt &\approx S(t_i, t_f) \\ &= \frac{h}{3} \left(f_0 + 4f_1 + \sum_{j=1}^{s/2-1} [2f_{2j} + 4f_{2j+1}] + f_s \right). \end{aligned} \quad (15)$$

Here f_n corresponds to the value of $\sum_j R_j(\mathbf{x}_n)$ at the time $t_n = t_i + nh$.

Nevertheless, our task is not to approximate the integral over a given interval, but to find the upper limit satisfying duplication condition (14). Furthermore, as we will describe in Sec. IV, this have to be repeated millions of times in a single simulation. Considering this, we implemented an efficient algorithm to estimate the value of t_d . Let S_T be an approximation to the value of the definite integral in Eq. (13), calculated by summing a number of approximations S over consecutive sub-intervals within t_0 to t . We start by calculating sequential approximations S using a broad integration range and time step until the cellular volume exceeds its duplication value

$$S_T > \ln 2. \quad (16)$$

Once in the vicinity of t_d , a couple of refining stages repeatedly cut in half both the integration range and time step until (14) is satisfied within a certain tolerance ϵ defined as

$$\left| \alpha \int_{t_0}^{t=t_d} \sum_j R_j(\mathbf{x}) dt - \ln 2 \right| < \epsilon. \quad (17)$$

IV. THE EVOLUTIONARY PROCESS

The *mutation-selection* process is a simple stochastic mechanism applied to groups of cells that results in successive modifications of the corresponding reaction networks in favor of faster cellular growth. During this process, the reaction network of a cell can be modified by adding a new edge between two randomly selected nodes. This action is called a *mutation*.

It is important to note that we distinguish between the time evolution of the chemical species inside the cell, as

described in Sec. II, and the changes on the structure of the internal network of the cells as they evolve. As already mentioned, in real life, the evolution of intracellular chemical species until binary fission takes from minutes to thousands of hours. On the other hand, a mutation could take several thousands of years to prevail. With such dramatic time differences it is impossible to use real time to trace the evolution of cellular networks. Therefore, we use the approach described in Ref. [17] and our *event time* will be given by changes in the network topology through the mutation-selection process, as described below.

This process begins with $m = 2N$ initial cells that share an identical internal state \mathbf{x}_0 , but whose graphs are generated by different mutations to a given initial network. These m cells are allowed to evolve in time, and their growth rate is estimated as described in Sec. III. Then, the n cells with the highest growth rate are selected to be the *mothers* cells of the first *generation*. Each generation is conformed by a set of $n \times m$ *daughter* cells. The network of a given daughter cell is generated as a mutation of one of the mothers. This is done m times for each of the n mother cells. Consistently with the fact that a daughter cell is not an exact replica of its mother, the daughters inherit as initial conditions the internal state of its mother at the duplication time plus a tiny perturbation on the values of the chemical concentrations. Subsequently, daughter cells are allowed to evolve, and growth rate is estimated. The n ones growing faster up to division are selected to be the mothers of the next generation, and so on.

This process is illustrated in Fig. 1.

Let us end this section by emphasizing the underlying computational difficulties involved in our study. As mentioned before, a large number N of chemical species must be considered and we follow the mutation-selection process for at least $4N$ generations, each of which consist of a set of $n \times m$ cells. For a typical simulation this requires to numerically solve millions of systems of nonlinear coupled ordinary differential equations including hundreds of variables. Besides the obvious requirement of the parallelization of the computation, it was also necessary to optimize the different algorithms as well as design an efficient flow structure for the whole simulation. Nevertheless, this efficiency can cause spurious results that must be brought under our control. For instance, for a given set of N nodes, the maximum possible *node degree* (number of paths linked to a node) is $k_S = N - 1$, i.e., when it is connected to every other node. This way, for a node with degree k , there remain $N - 1 - k$ possible mutations to be added. As the degree approaches k_S , the probability of the corresponding node being chosen from the mutations list is significantly reduced. We call this effect *high-degree saturation*. Fortunately, in most cases this saturation threshold k_S is high enough to cause no concern. Our implementation takes advantage of this and effectively reduces the execution time from $O(n^2)$ to $O(n)$ by lowering the saturation threshold to $(N - 1)/2$

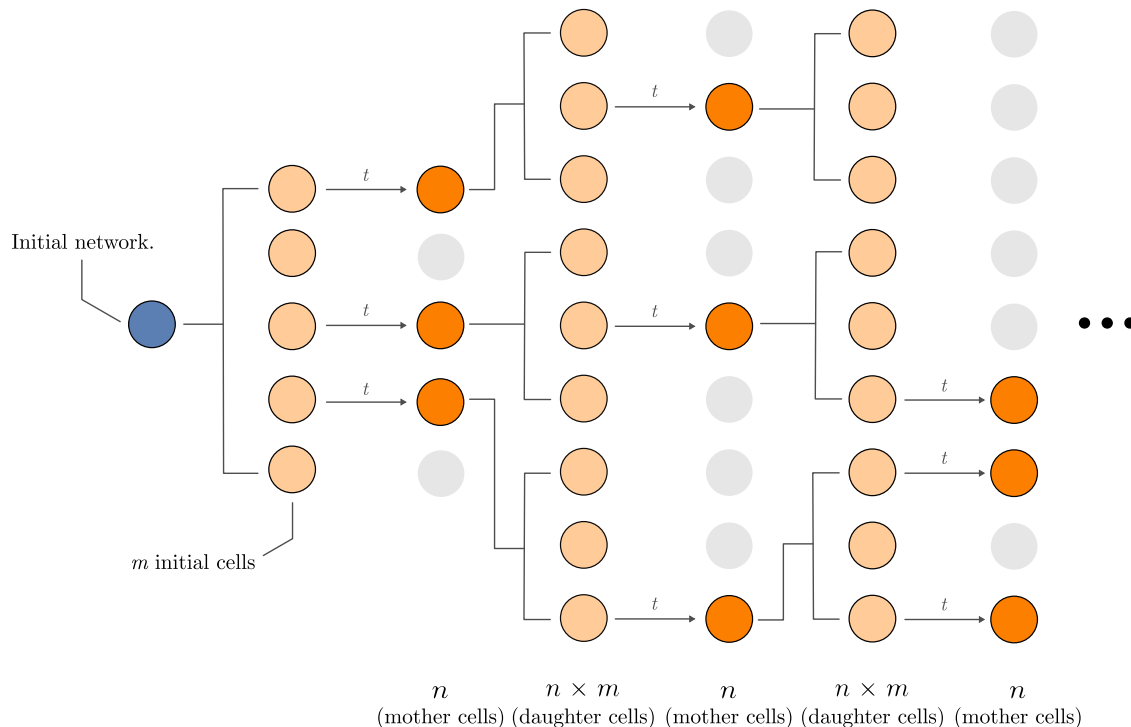


FIG. 1. Mutation-selection process diagram. Columns of light orange circles represent the set of $n \times m$ daughter cells of each generation.

or less. This is done by restricting the sample space of the possible mutations to the links of a complete (or near complete) random oriented graph, which is generated as a template prior to the execution of the simulation. Nevertheless, as saturation happens it can be easily identified because the degrees statistics will follow the Gaussian distribution of the corresponding template graph. This will be reflected as a characteristic peak centered at the average node degree $\langle k \rangle = \langle k_{initial} \rangle + g/N$, where g is the current generation (see Fig. 2). Therefore, in our imple-

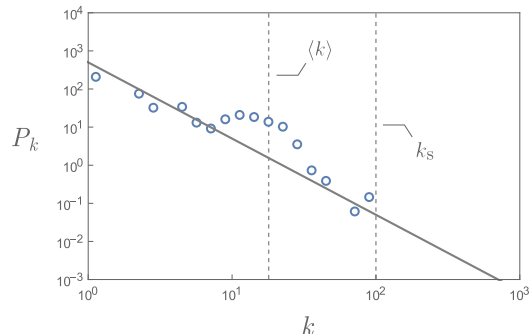


FIG. 2. Characteristic peak in the degree distribution in the spurious case of high-degree saturation. Here we show a network with $N = 500$ and $\langle k_{initial} \rangle = 1$ at the generation $g = 5000$. The saturation threshold was set at $k_s = 100$. The solid line represent a power-law with exponent -2 .

mentation, we are dictating the asymptotic outcome of

our mutation-selection process, though not the way it is reached. For all the simulations that we discuss in the following section, we follow closely the maximum degree of the nodes reached after each generation to make sure it is sufficiently under the saturation threshold. This gives us a number of reliable generations for a given simulation. Furthermore, it is worth emphasizing that for each simulation we generate a different template graph.

V. RESULTS

The results to be presented in this section were obtained using four nutrients, the external nutrient concentration $X_i = 0.2$, the diffusion coefficient $D = 4$, and the number of mother and daughter cells for each generation to be $n = 10$ and $m = 2N$, correspondingly (where N is the number of species). These values are borrowed from Ref.[12], where it is claimed that their results are robust with respect to variations of the model and simulation parameters. Furthermore, we choose the initial values for the concentrations randomly, but such that $\alpha = 1$ in Eq. (11), with random perturbations of the order of 10^{-6} for the concentrations inherited by the daughters. Finally, we set $\epsilon = 10^{-5}$ in Eq. (17) for the tolerance in the estimation of the cell duplication time.

As a first result it is convenient to mention that most of our outcomes were found to be independent of the number of chemical species, for N sufficiently large. Taking this into account, we often generalize their display by la-

belling them using the number of nodes N , which in our simulations took the values 250, 500 and 1000.

A. Degree of connectivity

As initial configuration for our simulations, we used random networks in three different connectivity regimes around the critical connectivity point. At this point a network has an average degree of $\langle k \rangle = 1$, i.e., the average number of edges per nodes is one. In the sub-critical regime ($\langle k \rangle < 1$) consist of small sub-networks isolated from each other, while in the super-critical regime ($\langle k \rangle > 1$) are characterized by the existence of a dominant large-sized sub-network known as *giant strongly connected component* (GSCC). Besides $\langle k \rangle = 1$, we also consider graphs with an initial average degree of $\langle k \rangle = 0.5$ and $\langle k \rangle = 4$. Note that in all three cases, the connectivity stays below the threshold for fully connected random directed graphs, $\langle k \rangle = \ln N$ [18].

Since we start with random networks, at the beginning of the simulations both, the in- and out-degree distributions, obey binomial laws, as observed in Fig. 3(a) [19]. Afterwards, we found that the behavior of the topology of the graphs during the mutation-selection process strongly depends on the initial connectivity of the networks. In general, it is observed that by the N -th generation the degree distribution already shows a well defined pattern. In the cases starting with a low connectivity ($\langle k \rangle = 0.5, 1.0$), the degree distribution is described by a power-law with an exponent near -2 , as seen in Fig. 3(b). This value signals the emergence of a hub-and-spoke network where the hubs are in contact with a large fraction of all nodes [1]. For these cases, as the simulation continues, the size and number of hubs increase, extending the distribution toward higher connectivities. The functional form of the distribution is maintained during the rest of the mutation-selection process as seen in Figs. 3(c)-3(f). On the other hand, the degree distribution developed in the cases that started with a high connectivity ($\langle k \rangle = 4$) deviate from a pure power-law, showing a low-degree cutoff below a certain k_{min} , as observed in Fig. 4. This behavior is not shown in analogous simulations (using $\langle k \rangle = 4$) previously conducted by Furusawa and Kaneko [12]. Yet, these authors report a power-law distribution with an exponent near -3 , which in turns agrees with a fit restricted to the scaling region observed in our simulations. As explained in Ref. [1], in the case of a pure power-law with exponent -3 , hubs with the largest degree of connectivity are linked to a small fraction of all nodes, which is to be contrasted with the case with exponent -2 described above. Noting that $\langle k \rangle = 4$ is rather close to $\ln N$, the full connectivity threshold for a random directed graph, we performed one more simulation with an intermediate initial connectivity of $\langle k \rangle = 2$. We found its behavior to be qualitatively the same as the one obtained for low initial connectivity, with a degree distribution that follows a power-law with an exponent

near -2 .

Our results suggest that the evolution observed for $\langle k_{initial} \rangle = 4$ is not distinctive of the mutation-selection process, but rather an artifact of a particular setup that imposes constraints on the graph topology. Since nodes can only gain connections and there is a fixed number of nodes, a random network with a high initial connectivity directly limits the amount of possible low-degree nodes during a simulation, leading to the observed cutoff in the low connectivity region. Even if this behavior is consistent with a wider definition of the scale-free property, the excellent fit to a pure power-law of the degree distribution of real metabolic networks [20] should discourage the use of highly connected initial states. Even more, if we identify connectivity with complexity, it makes more sense, from an evolutionary perspective, to start from simple cells and evolve into more complex ones.

B. Small world structure

One universal characteristic of complex networks is that they usually describe *small-worlds*. In these networks the distance between any pair of nodes, no matter how disconnected they seem to be, is usually considerably shorter than naively expected. In graph theory, the distance between two nodes is measured as the number of edges in the shortest path that connects them. The *average minimum distance* among all pairs of nodes, $\langle d \rangle$, characterizes the overall network interconnectivity, and in general it quantifies the flux or transmission efficiency of the system. In the context of a metabolic network, $\langle d \rangle$ indicates the average length of the shortest pathway between every pair of metabolites. In a small-world it is known that, for graphs with similar degree of connectivity, the average minimum distance satisfies $\langle d \rangle \sim \ln N$. This implies that $\langle d \rangle$ depends slightly on network size, a characteristic typically observed in the structure of metabolic networks [21].

When studying the connectivity properties of sparse networks, as our modeled cells, it is useful to describe exclusively the GSCC, as it reflects the connectivity of the whole network [22]. Taking into account the results in the previous section, from now on we consider simulations that started with a connectivity $\langle k \rangle = 1$. Therefore, as already mentioned, after a few mutations there should arise a GSCC. We verified that this indeed happened in our simulations. Taking this into account, to study the behavior of $\langle d \rangle$ we follow the evolution of the GSCC of three networks with $N = 250, 500$ and 1000 nodes, respectively. Then we determine the mean and standard deviation of $\langle d \rangle$ for these cases. Even if this sample of three cases is poor, Fig. 5 allows us to conclude that the mutation-selection process leads to small-worlds, because it is observed that the standard deviation decreases drastically with the pass of the generations, while the average minimum distance converges to a value around 4 independently of the network size in an comparable number

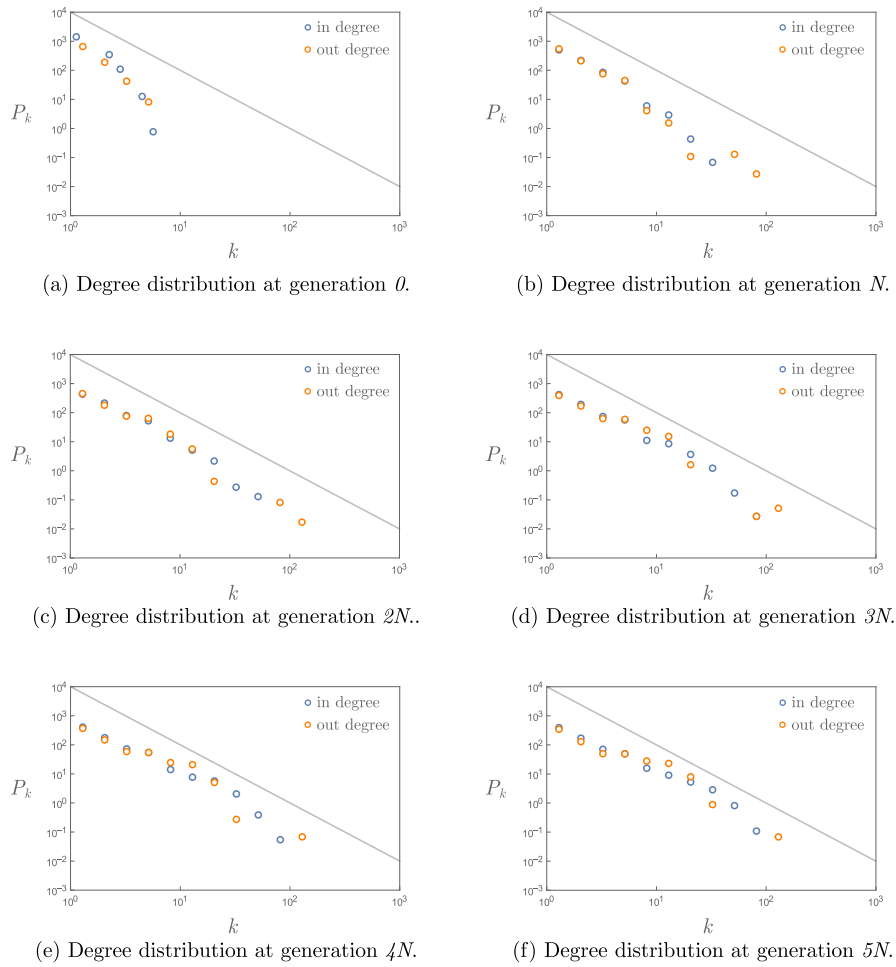


FIG. 3. Evolution of the in- and out-degree distributions. Here we show the results from a 1000 nodes network with $\langle k_{initial} \rangle = 1$. The solid line represents a power-law with exponent -2 .

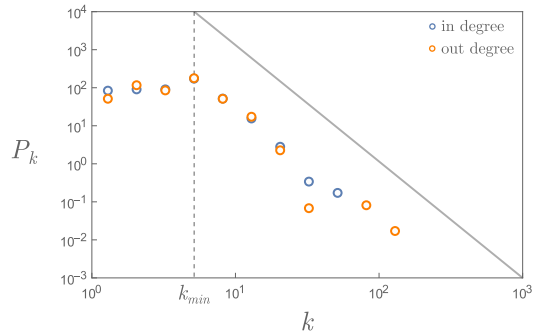


FIG. 4. Degree distribution of a network at generation $2N$ starting off with a configuration with $\langle k \rangle = 4$. The solid line represents a power-law with exponent -3 . The dashed line indicates the value of k_{min} . Here we show the results for a network with 1000 nodes.

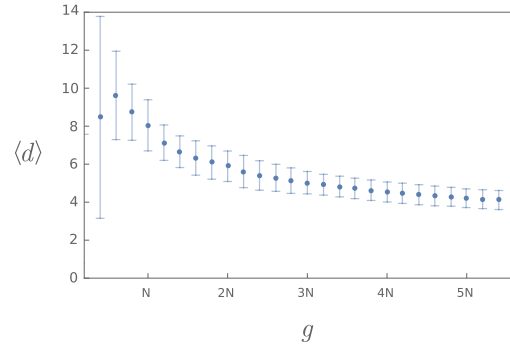


FIG. 5. Evolution of the mean and standard deviation of the average minimum distance ($\langle d \rangle$) during the mutation-selection process of different simulations with network sizes varying from 250 nodes up to 1000 nodes. The initial configuration for all simulations is a random network with $\langle k \rangle = 1$.

of generations (parameterized in the figure by N). Notice that the asymptotic value for $\langle d \rangle$ is remarkably close to those from real metabolic networks, which fall in the interval from 2 to 5, depending on the organism [21].

C. Central species

While the average minimum distance provides a large-scale characterization of the network, *centrality* measures provide information about specific nodes that play an important role in the overall network dynamics. Here we are going to focus on the *closeness centrality*, which for a node is defined as the inverse of its average minimum distance from every other node. In the case of directed networks the closeness centrality can be measured both inwardly and outwardly from the nodes. Through this parameter it is possible to objectively identify the central metabolites on a metabolic network [23]. Centrality analysis helps to understand the metabolic system not only at a structural level, but at the base of its functional organization, providing additional clues about the mechanisms that shape the networks as they evolve.

As shown in the right panels of Fig. 6, in our simulations nodes corresponding to nutrient species developed the highest outward closeness centrality, followed by randomly distributed nodes. This result can be explained by the fact that, if by chance any other non-nutrient species gets involved as substrate in a large number of reactions, these reactions will stop after the given species is exhausted. In contrast, if the inner nutrients concentrations decline, a gradient with respect to the external nutrients concentrations builds up, which leads to an increase in nutrient intake from the environment.

On the other hand, in the left panels of Fig. 6, we observe that the carrier species developed the highest inward closeness centrality. This seems to happen several generations after the nutrients dominated the outward centrality, implying that, at this point of the evolution, when the connectivity of the graph has grown significantly, the above mentioned induced gradient seems to no longer be sufficient to sustain the nutrient intake from the environment needed for the reactions. This problem is henceforth solved for those cells with networks able to yield higher concentrations of nutrient carriers.

Within the limitations of the catalytic reactions model stated in Sec. II, these results are compatible with what is known for the metabolic networks of living organisms [22].

D. Hierarchical structure

A wide variety of real systems present networks that can be subdivided into *modules*, weakly interacting subsets of strongly interconnected nodes. Modules had attracted a lot of interest because they are typically associated with specific system functions. The development and optimization of algorithms for module detection in large networks is currently one of the main challenges for graph theory, due to the extensive computational requirements and the selection of the search criteria. Some examples of these search criteria are the modularity maximization and the suppression of high centrality links,

which respectively correspond to the Greedy and Girvan-Newman algorithms [24].

The existence of a hierarchical structure in networks from both natural and artificial systems is a fact [25]. These structures consist of modules constituted by smaller sub-modules in a recursive fashion. This property is reflected in the distribution of the *clustering coefficient* of the network nodes behaving as $C_k \sim k^{-1}$. Taking this into account, it is possible to detect quantitatively the presence of a hierarchical structure on a network [26]. In particular, this is the behavior observed in metabolic networks [1].

Our analysis of the networks resulting from the mutation-selection process reveals a different behavior; C_k is mainly independent of the node degree, as observed in Fig. 7. At an early stage of the evolutionary process, this behavior is expected, because of the properties of the Erdős-Reyni random network model. Nevertheless, we found that the mutation-selection mechanism have little effect on this behavior. To some extent, this is also to be expected owing to the similarity of the mechanism considered here to the more general Albert-Barabási preferential attachment model, where the clustering distribution is also independent of the node degree [17, §9.3 *Hierarchical Clustering*].

E. Intracellular species concentration

The results presented in the previous subsections give us a good idea of how the topology of the graph representing a cell varies as dictated by the mutation-selection process. Topology determines the general pattern of a cell metabolism, but even for a fixed graph, the particular realization of the evolution of the internal cellular state depends on the initial conditions for Eqs. (10). Then, it is interesting to determine what is universal in the intracellular dynamics as it changes during the evolutionary process.

In all considered cases, starting from a random internal state, after a relatively small number of generations, a scaling region arises in the ranking distribution of the intracellular concentrations. This region is fairly described by a power-law distribution. And, as observed in Fig. 8, it widens as the simulation proceeds. Nevertheless, a well defined cutoff in the low concentration region is always present. This is consistent with the results previously reported by Kaneko and Furusawa (2006) for a similar simulation [12].

A deeper analysis revealed a positive correlation between concentrations and the overall node connectivity, as observed in Fig. 9. This correlation is developed over the course of the simulation, becoming distinct for the set of nodes ranked with higher overall connectivity. We have found that, in general, this set comprises between 20 and 30 percent of the graph nodes. We labeled the corresponding subgraph as *core*. It starts by being disconnected, but becomes weakly connected around

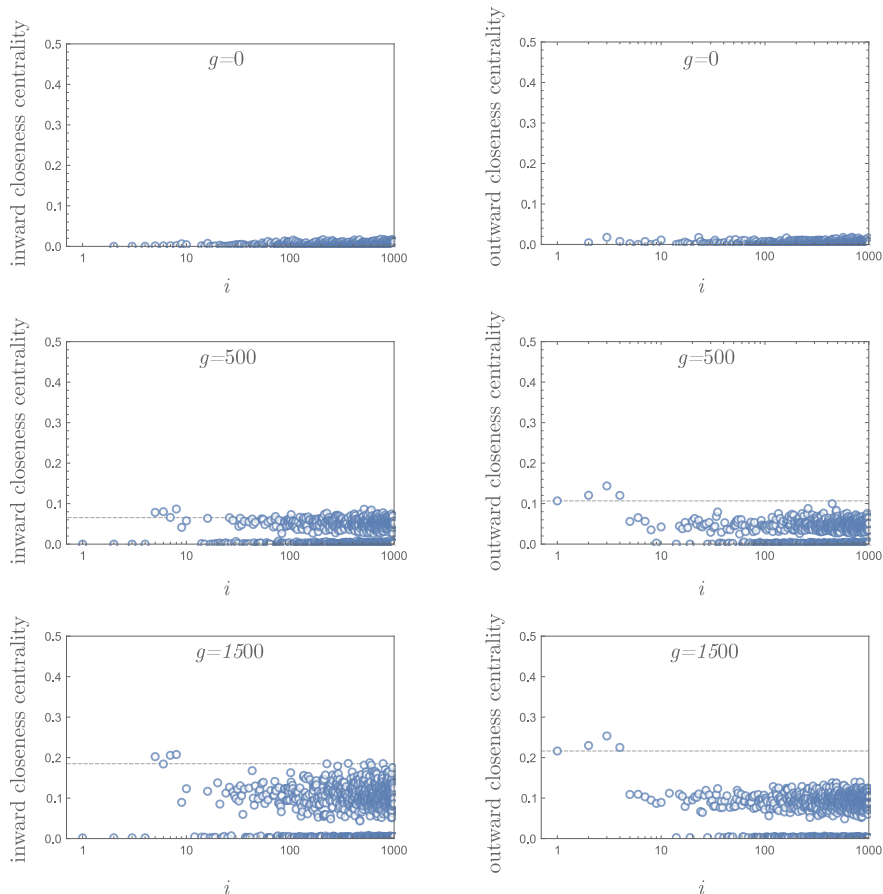


FIG. 6. Evolution of the inward (left column) and outward (right column) centrality of the nodes during the mutation-selection process with a 1000 nodes network. The first four nodes correspond to nutrient species and the following four are their respective carriers.

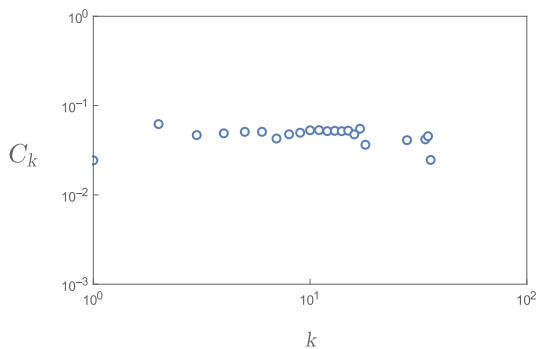


FIG. 7. Typical clustering distribution of the networks during the simulations. Here we show the distribution of a 250 nodes network after 1250 generations.

the $1.5N$ generation, while the core complement remains disconnected the whole simulation. The core is almost completely contained in the GSCC of the whole network as represented in Fig. 10. The nodes that are in the core but not on the GSCC mostly correspond to nutrient species, which by definition cannot be in a strongly connected component. Following exclusively the behav-

ior of the concentrations in the core, it is observed that their ranked distribution reaches a stable pure power-law with an exponent near -1 around the $2N$ generation [27]. This is illustrated in Fig. 11.

As we noted in Sec. VB, the evolution of the whole network into a small-world structure can be completely determined by the changes in the GSCC. Here we find that the main functional characteristics of the cell are dictated by the nodes in the core. Moreover, the structure presented in Fig. 10 resembles the connectivity structure of real metabolic networks found in Ref. [22].

VI. SUMMARY AND DISCUSSION

The results presented in the previous section are summarized in the evolutionary timeline shown in Fig. 12. Let us delineate the process, recalling first that we have found that the number of generations at which the main phases of the evolution take place can be parametrized by N , the number of species in the modeled cells (in particular N taking here the values 250, 500 and 1000).

In the beginning, i.e., at $0N$ generations, cells were

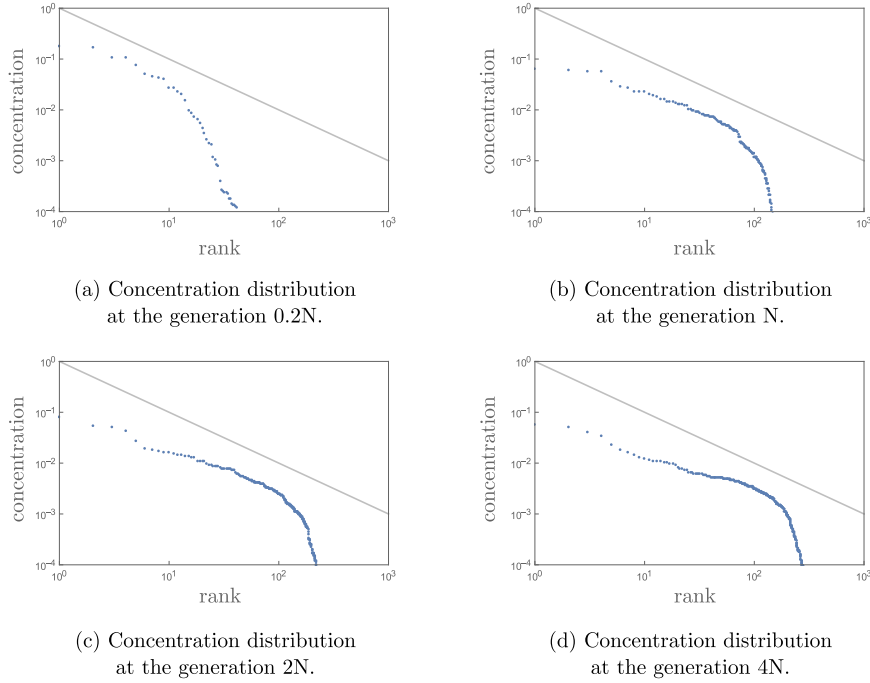


FIG. 8. Evolution of the intracellular chemical concentration distribution over the course of a simulation. This distribution is built after ranking the species from highest concentration to lowest concentration. The solid line corresponds to a power-law with exponent -1 . Here we show the result for a network with $N = 500$ nodes.

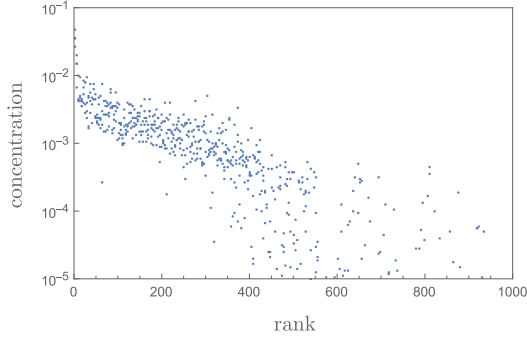


FIG. 9. Correlation between nodes degree and intracellular concentration. Here the different species are ranked according to its node overall degree. These concentrations in particular correspond to a 1000 nodes network at the generation $g = 4000$.

considered to be random networks. The idea of randomness as a precursor of life can be traced back to the pioneering works of Kauffman, whose theories centered on properties of random directed graphs [28]. Several other mathematical models have shown that a primitive metabolic system can arise from a stochastic configuration of inanimate elements [9, 29]. Following this line, in this work we have shown that from a primordial cell, modeled as a random set of catalytic reactions, a self-reproducing system can arise in a Darwinian process of mutation and selection that favours cells with the highest replication rate. As we will see, we found a better corre-

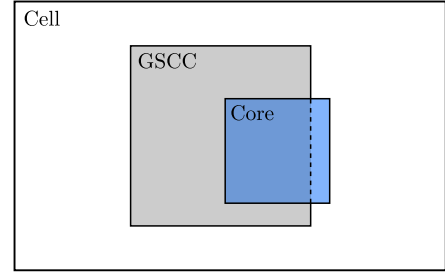


FIG. 10. Illustrative Venn diagram showing the sets of nodes in the whole network (white rectangle), the giant strongly connected component (gray rectangle) and the core (blue rectangle).

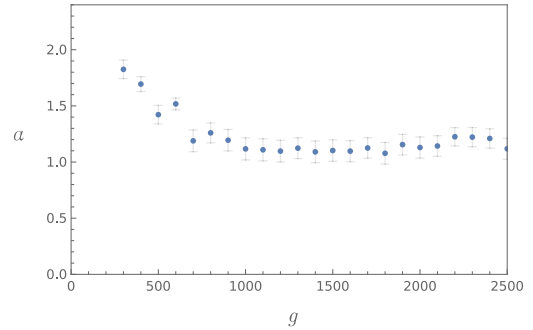


FIG. 11. Evolution of the exponent of the power-law distribution for the core. Gray bars denote the fit error. It is shown the result for a 500 nodes network.

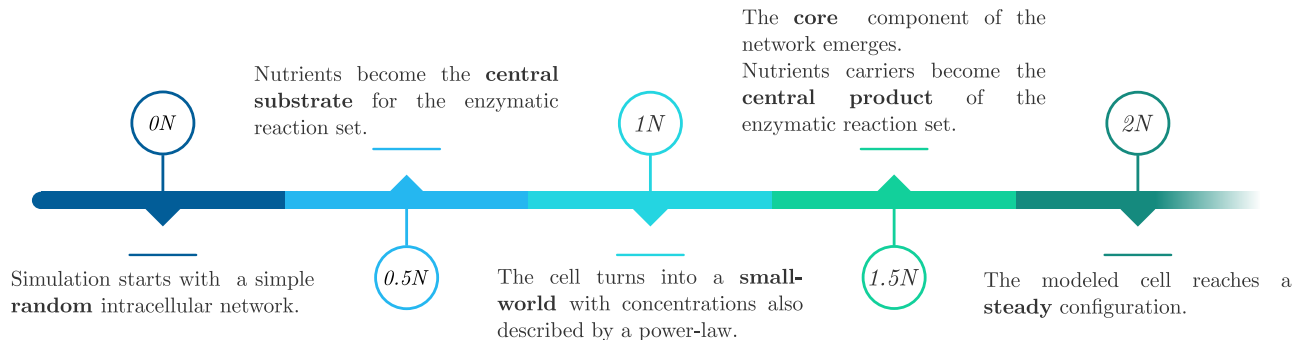


FIG. 12. Timeline of a modeled cell during the mutation-selection process.

spondence with observational data when the initial cell is constituted by a rather small number of catalytic reactions. From an evolutionary perspective, it implies starting from simple cells and evolving via mutation-selection dynamics into more complex ones.

After the simulation is set up, the first distinct signal of organization appears by the $0.5N$ -th generation, when nodes corresponding to nutrient species achieve the highest outward centrality among all nodes. This means that, at this stage, the mutation-selection mechanism picks up cells shortening metabolic pathways that link nutrients to every other species. Bearing in mind that in our simple model only the species permeated from outside the cell (i.e., the nutrients) act as precursors for the synthesis of the rest of the species, our result is in agreement with the one found for the metabolic networks of living organisms, where the dominant ‘outward’ central metabolites correspond mainly to building-block molecules. For example, in the case of the metabolic network of the *Escherichia coli*, the top ‘outward’ central metabolites correspond to pyruvate and acetyl-CoA, along with other intermediary metabolites [22].

Around the $1N$ -th generation of the simulation, the degree distribution of the cellular networks gets described by a power-law (coming from an initial binomial distribution). This indicates the emergence of the scale-free structure universally associated with the so-called *small worlds*. Such connectivity is one of the main structural characteristic of real metabolic networks, and have been linked to the ability of the cell metabolism to rapidly react to both internal and external perturbations [23, 30]. We have found that to obtain a pure power-law for the degree distribution of a modeled cell, as observed in real metabolic networks [20], it is convenient to start the simulation with a low degree of connectivity. This is suitable for describing the evolution of a cell which starts as a set of elementary and mostly independent chemical reactions and, while competing to be the fittest one, becomes more complex with every passing generation,

exhibiting a richer structure of interconnected enzymatic reactions. It is important to note a key difference in the interpretation of the scale-free property in our study with respect to that discussed in Albert-Barabási works based on the preferential attachment model of scale-free networks [17]. According to the latter, it is hypothesized that in a metabolic network the highly connected metabolites should be the oldest phylogenetically, which is well supported by experimental analysis [23]. Nevertheless, in the catalytic reaction network model there is no temporal distinction among nodes, thus, the highly connected ones arise solely by their functional roles in the reaction network, displaying a complementary mechanism by which such hub nodes can develop. With regard to this point, it is also worth noting that the emergence of the power-law for the degrees distribution coincides with the rise of a scaling region in the ranked concentrations distribution described also by a power-law. As mentioned, this kind of behavior is an universal fingerprint of the intracellular chemical composition of living organisms [21, 31].

Near the $1.5N$ -th generation, the subgraph of the nodes with the highest connectivity degree becomes connected, indicating the emergence of a tightly connected *core* component in the network. This is consistent with the fact that, for many living cells, there is a small number of keys metabolites (a few dozens) that exhibit the highest degree of connectivity [22, 23]. Interestingly, we also found that, at this stage, the nodes belonging to this core mostly correspond to those species exhibiting the highest concentrations. The key functional role of the core in the modeled metabolism is highlighted by the fact that the subgraph which complements the core in the network remains disconnected throughout the whole evolution. In this regard, it should be mentioned that using exclusively a criterion based on the clustering distribution, in our modeled cell we did not find the structure of nested subnetworks typical for the metabolism of living cells [32]. Nevertheless, this key difference has

been observed before in similar processes where a network is gradually modified, particularly, in the Albert-Barabási preferential attachment model [17]. Besides using another algorithms to search for hierarchical structure, it motivates us to study modifications of the model to include, for example, cost of maintenance of metabolic pathways and to simulate cellular adaptation to a given environment along with the cellular growth optimization. These mechanisms had been directly associated with the development of a hierarchical structure in bacterial metabolic networks [3]. Back to the functional role of the core, it is important to note that this is the same evolutionary phase when the nutrient carriers finally become central as product of the chemical reactions. This seems to differ from what it is reported in Ref.[22], where it was found that the top most ‘inward’ central metabolites in the *Escherichia coli* metabolic network correspond to the same intermediary metabolites dominating the outward centrality. Most of these metabolites are part of the so-called ‘central metabolism’, namely the glycolysis and tricarboxylic acid cycle pathways. One reason for the apparent discrepancy between their and our results is that in our model the ‘catabolic-like’ reactions which could lead to this behavior, are deliberately excluded by restricting nutrients from being product of any reaction. Recall that this constraint is enabled here because we do not aim to recreate the inner cellular dynamics on the whole, but rather to focus solely on the traits leading to steady cell growth. Nonetheless, this restriction in the model reveals the key role of the carrier species in the self-regulation mechanism of the cells during the mutation-selection process. As a consequence of evolutionary pressure in favor of a faster growth rate, mutations to the cells that promotes a more efficient nutrient consumption and transformation prevail. In our simulations this is directly reflected in the fact that the outward closeness centrality ended dominated by the nutrients species. Still, in order to maintain such an optimal growth rate, the needed nutrient supply for the remaining species must be preserved by an equally efficient nutrient inflow from outside the

cell, which in this model is regulated solely by the carrier species. We believe this is the reason why they end dominating the inward centrality. Since the carriers are part of the core, the fact that this happens concurrently with the emergence of the core is unlikely to be a coincidence.

Within the constraints of our simulation, the final stage of the evolution of the modeled cell is found to start around generation $2N$, when the exponent in the power-law distribution describing the concentrations probability for the core reaches an stable value very close to -1 . This case, corresponding to what is known as Zipf’s law, is special because is ubiquitous in systems where inner competition lead to changes in their components size, either by aggregation or fracture. Such a simple scaling in the ranked probability distributions has been observed in a broad range of domains like word frequencies in a text, city and firm sizes, incomes, amino acids sequences, neural activity, hub traffic and social contacts networks. This pervasive presence of the Zipf’s law is expected to be related with a fundamental and universal mechanism for emergence of complexity [33]. For our simulation, since the core component seems to dictate the performance of the whole cell, the fact of settling down into this steady state implies that a configuration is reached when new mutations not longer impact the reaction kinetics supported by the inner structure of our modeled cell. This could be an instance of the ‘cost of complexity’ hypothesis [34] at cellular level.

VII. ACKNOWLEDGMENTS

We thank Andrea Rodríguez, Paulina González, Roberto Sáenz and Sara Centeno for their useful discussions. We also acknowledge HypernetLabs and Google Cloud Services for allowing us to use their computational facilities to run most of our simulations. The work of D. R-O was supported by a CONACyT grant for graduate studies.

-
- [1] A.-L. Barabási and Z. N. Oltvai, Network biology: Understanding the cell’s functional organization, *Nature Review Genetics* **5** (2004).
 - [2] M. Penedo, K. Miyazawa, N. Okano, H. Furusho, T. Ichikawa, M. S. Alam, K. Miyata, C. Nakamura, and T. Fukuma, Visualizing intracellular nanostructures of living cells by nanoendoscopy-afm, *Science Advances* **7** (2021).
 - [3] A. Goodman and M. Feldman, Evolution of hierarchy in bacterial metabolic networks, *BioSystems* **180** (2019).
 - [4] Y. Bromberg, A. A. Aptekmann, Y. Mahlich, L. Cook, S. Senn, M. Miller, V. Nanda, D. U. Ferreira, and P. G. Falkowski, Quantifying structural relationships of metal-binding sites suggests origins of biological electron transfer, *Science Advances* **8** (2022).
 - [5] S. Ameta, Y. J. Matsubara, N. Chakraborty, S. Krishna, and S. Thutupalli, Self-reproduction and darwinian evolution in autocatalytic chemical reaction systems, *Life* **11** (2021).
 - [6] S. A. Benner, Defining life, *Astrobiology* **10** (2010).
 - [7] S. Kauffman, Homeostasis and differentiation in random genetic control networks, *Nature* **224** (1969).
 - [8] S. A. Kauffman, Metabolic stability and epigenesis in randomly constructed genetic nets, *Journal of Theoretical Biology* **22** (1969).
 - [9] A. Filisetti, M. Villani, C. Damiani, A. Graudenzi, A. Roli, W. Hordijk, and R. Serra, On raf sets and autocatalytic cycles in random reaction networks, *Advances in Artificial Life and Evolutionary Computation* (2014).
 - [10] S. Jain and S. Krishna, Autocatalytic sets and the growth of complexity in an evolutionary model, *Phys. Rev. Lett.*

- 81** (1998).
- [11] K. Kaneko and T. Yomo, Isologous diversification: A theory of cell differentiation, *Bulletin of Mathematical Biology* **59** (1997).
- [12] C. Furusawa and K. Kaneko, Evolutionary origin of power-laws in a biochemical reaction network: Embedding the distribution of abundance into topology, *Physical Review E* **73** (2006).
- [13] C. Furusawa and K. Kaneko, Origin of complexity in multicellular organisms, *Physical Review Letters* (2000).
- [14] C. Furusawa and K. Kaneko, Chaotic expression dynamics implies pluripotency: when theory and experiment meet, *Biology Direct* (2009).
- [15] C. Furusawa and K. Kaneko, Formation of dominant mode by evolution in biological systems, *Physical Review E* **97** (2018).
- [16] C. Furusawa and K. Kaneko, Emergence of rules in cell society: Differentiation, hierarchy, and stability, *Bulletin of Mathematical Biology* **60** (1998).
- [17] B. Albert-László, *Network Science* (Cambridge University Press, 2016).
- [18] I. Palásti, On the strong connectedness of directed random graphs, *Studia Scientiarum Mathematicarum Hungarica* **1** (1966).
- [19] Plots were built using logarithmic binning to correct for the sampling bias introduced by a typical lineal binning (see Ref. [17], §4.12 *Advanced Topic 3.B: Plotting Power-laws*).
- [20] A. D. Broido and A. Clauset, Scale-free networks are rare, *Nature Communications* **10** (2019).
- [21] H. Jeong, B. Tombor, R. Albert, N. Oltvai, and A. Barabási, The large-scale organization of metabolic networks, *Nature* **407** (2000).
- [22] M. Hong-Wu and Z. And-Ping, The connectivity structure, giant strong component and centrality of metabolic networks, *Bioinformatics* **19** (2003).
- [23] A. Wagner and D. A. Fell, The small world inside large metabolic networks, *Proceedings of the Royal Society B: Biological Sciences* **268** (2001).
- [24] A. Clauset, M. E. J. Newman, and C. Moore, Finding community structure in very large networks, *Physical Review E* **70** (2004).
- [25] B. Corominas-Murtra, G. Joaquín, R. Solé, and C. Rodríguez-Caso, On the origins of hierarchy in complex networks, *PNAS* **110** (2013).
- [26] E. Ravasz and A. L. Barabási, Hierarchical organization in complex networks, *Physical Review E* **67** (2003).
- [27] The exponent is found using the Python library `plfit.py`, an implementation by Adam Ginsburg of the general algorithm presented by Clauset et al. (2009) [35].
- [28] S. Kauffman, Autocatalytic sets of proteins, *Journal of Theoretical Biology* **119** (1986).
- [29] M. Steel and E. Mossel, Random biochemical networks: the probability of self-sustaining autocatalysis, *Journal of Theoretical Biology* **233** (2004).
- [30] D. J. Watts and S. H. Strogatz, Collective dynamics of ‘small-world’ networks, *Letters to Nature* **393** (1998).
- [31] S. Sato, M. Horikawa, T. Kondo, S. T, and M. Setou, A power law distribution of metabolite abundance levels in mice regardless of the time and spatial scale of analysis, *Scientific Reports* (2018).
- [32] E. Ravasz, A. L. Somera, D. A. Mongru, Z. N. Oltvai, and A. L. Barabási, Hierarchical organization of modularity in metabolic networks, *Science* **297** (2002).
- [33] M. Cristelli, M. Batty, and L. T. Pietronero, There is more than a power law in zipf, *Scientific Reports* **2** (2012).
- [34] H. A. Orr, Adaptation and the cost of complexity, *Evolution* **54** (2000).
- [35] A. Clauset, C. R. Shalizi, and M. E. J. Newman, Power-law distributions in empirical data, *SIAM Review* **51** (2009).